Intra-atomic Electron-Electron Scattering in p-He Collisions (Thomas Process) Investigated by Cold Target Recoil Ion Momentum Spectroscopy

V. Mergel,[1,*] R. Dörner,[1] M. Achler,[1] Kh. Khayyat,[1] S. Lencinas,[1] J. Euler,[1] O. Jagutzki,[1] S. Nüttgens,[1] M. Unverzagt,[1] L. Spielberger,[1] W. Wu,[2,†] R. Ali,[2,‡] J. Ullrich,[3] H. Cederquist,[4] A. Salin,[5] C. J. Wood,[6] R. E. Olson,[6] Dž. Belkić,[4] C. L. Cocke,[2] and H. Schmidt-Böcking[1]

[1]*Institut für Kernphysik, Universität Frankfurt, August-Euler-Strasse 6, D-60486 Frankfurt, Germany*

[2]*Kansas State University, Manhattan, Kansas 66506*

[3]*Gesellschaft für Schwerionenforschung mbH, Planckstrasse 1, D-64291 Darmstadt, Germany*

[4]*Atomic Physics, Stockholm University, Frescativ. 24, S-104 05 Stockholm, Sweden*

[5]*CNRS and Université Bordeaux, F-33405 Talence, France*

[6]*University of Missouri-Rolla, Missouri 65401*

(Received 26 February 1997)

We have performed a kinematically complete experiment for the transfer ionization reaction 0.15–1.4 MeV $p + \mathrm{He} \rightarrow \mathrm{H}^0 + \mathrm{He}^{2+} + e^-$ by measuring the three-dimensional momentum vector of the He^{2+} ion in coincidence with the scattering angle and the plane of the H^0. In the measured fourfold differential cross section we can clearly distinguish between the independent two-step process of capture plus ionization and the correlated e-e Thomas scattering. We find a $v_P^{-7.4\pm1}$ scaling for the total cross section of the e-e Thomas process. [S0031-9007(97)03631-4]

PACS numbers: 34.70.+e, 34.50.Fa, 39.90.+d

One of the fundamental capture mechanisms for fast ion atom collisions was proposed by Thomas in 1927 [1] based on a classical treatment. This Thomas process can be understood as two consecutive binary collisions; first, by the projectile with one of the target electrons and, second, between this electron and either the target nucleus (e-N Thomas scattering) or another target electron (e-e Thomas scattering). The e-e Thomas scattering offers a unique possibility for investigating the dynamic electron-electron (e-e) correlation in atomic collision processes. For fast proton impact the perturbation of the target (in our case, helium) is small, and the electrons are quickly removed from the bound state by the e-e Thomas scattering. Thus this process will leave the nucleus behind with its momentum distribution from the initial ground state, which mirrors the sum momentum of the two electrons. Furthermore, the absolute probability for that process yields information on the spatial distribution of the two electrons. The e-e Thomas scattering always leads to a double ionization of the target, while the capture can either be to a bound [transfer ionization (TI)] or a continuum state of the projectile [2].

Only two experiments [3,4] which tried to find evidence for this e-e Thomas process have been reported in the literature. Both observed significant structures in singly (Horsdal *et al.*) [3] and doubly (Palinkas *et al.*) [4] differential cross sections of the TI in proton-helium collisions. Horsdal *et al.* found a peak in the ratio of transfer ionization to total transfer (with and without ionization) at a scattering angle (θ_P) of about 0.55 mrad at projectile energies of $E_P = 0.2$–0.5 MeV. Gayet and Salin [5], however could reproduce this peak within an independent electron model (IEM). We experimentally confirm that this peak is caused mainly by the independent two-step process and not by the e-e double scattering. Palinkas *et al.* [4] found a peak in the doubly differential cross section $d^2\sigma/(dE_e d\Omega_e)$ at $\theta_e = 90°$ and $E_e = 600$ eV at $E_P = 1$ MeV, which could be reproduced by a second-order Brinkman-Kramers approximation (BK2) of Briggs and Taulbjerg [6], in contrast to the IEM [5]. For TI, Ishihara and McGuire [7] predicted electron emission along a second-order ridge at $\mathbf{k} + \mathbf{q} = 0$, where $\mathbf{k}$ is the momentum vector of the free electron, respectively, and $\mathbf{q}$ the momentum change of the projectile. The Thomas singularity should be located on that ridge at $k = v_P$, where v_P is the projectile velocity.

In this Letter we report on the first kinematically complete experiment for TI. We have measured all three momentum components of the recoiling He^{2+} ion, with a solid angle of nearly 4π, in coincidence with the polar and azimuthal deflection angle of the outgoing H^0 atom. These five momentum components fully determine the final state of the reaction (apart from the spin). The remaining four momentum components of the three particles in the continuum (H^0, He^{2+}, e^-) are determined by the energy and momentum conservation laws, assuming capture to the ground state [8]. We can clearly separate the independent two-step process from the second-order e-e Thomas scattering by their different locations in the nine-dimensional momentum space, and thus we can determine the contributions to the total TI cross section for each of them separately.

We have used cold target recoil ion momentum spectroscopy (COLTRIMS) [9–12] to determine the three-dimensional momentum vector and the charge states of the recoil ions. The projectile beam was collimated to a size of <0.5 mm and a divergence of <250 μrad. The beam was charge-state selected before and after the target region by

 © 1997 The American Physical Society

different sets of electrostatic deflector plates. A precooled supersonic helium gas jet was used as target. It combines the two most important features necessary for recoil ion spectroscopy: low internal temperature (<50 mK) and the localization of the target (diameter 5 mm). A residual gas pressure without a gas jet of 1×10^{-8} mbar and a target thickness in the jet of 1.5×10^{12} cm^{-2} were obtained. Recoil ions created in the interaction volume with the projectile beam were accelerated by a weak electric field (9 V/cm) onto a two-dimensional position sensitive channel-plate detector with wedge-and-strip readout. Instead of a homogeneous field, used in previous experiments [9–11], an electro-optical configuration which focuses the extension of the target region in all three dimensions on the detector was used [12]. This improves the momentum resolution by a factor of 10. For this experiment we ran the spectrometer with a momentum resolution of ± 0.15 a.u., less than the optimum resolution of ± 0.025 a.u. for all three directions, in favor of a higher target density.

The mechanisms responsible for nonradiative capture plus ionization can be grouped into two types, depending on whether (i) mainly the target nucleus or (ii) the continuum electron compensates the momentum change of the projectile, due to the mass transfer by the captured electron. Process (i) occurs if a target electron is captured by a projectile-target interaction due to a velocity matching between the electron and projectile involving the electronic velocity distributions in the initial and final bound state (kinematic capture), or if an e-N Thomas process occurs. From [13] we estimated that the e-N Thomas process is negligible for TI at the observed energies. To achieve TI in this process the second electron must also be emitted to the continuum. The second step might involve either a second interaction of the projectile with the target (IEM) [see Fig. 1(a)] or proceed via relaxation of the target wave function (shake-off). McGuire *et al.* proposed an exchanged order of the latter process with ionization and shake-over [14]. The e-e Thomas mechanism [see Fig. 1(b)] is a type (ii) process, which could, in principle, occur with two initially unbound electrons or, more generally, via the second-order ridge discussed by Ishihara and McGuire [7].

The determination of all nine momentum components allows us to distinguish experimentally between the independent process and the correlated e-e Thomas mechanism. For TI, momentum conservation reads

$$K_{x,y,z} = -(q_{x,y,z} + k_{x,y,z}), \tag{1}$$

where $K_{x,y,z}$ are the momentum components of the He^{2+}-recoil ion, $k_{x,y,z}$ of the emitted electron and $q_{x,y,z}$ the momentum change of the projectile. x, y denote the two components perpendicular and z the component parallel to the incident projectile. Using energy conservation, it follows to first order in Q/E_P and in the ratio between electron and projectile mass for the longitudinal (z) direction [12] [atomic units are used throughout ($e = \hbar = m_e = \alpha c = 1$)]

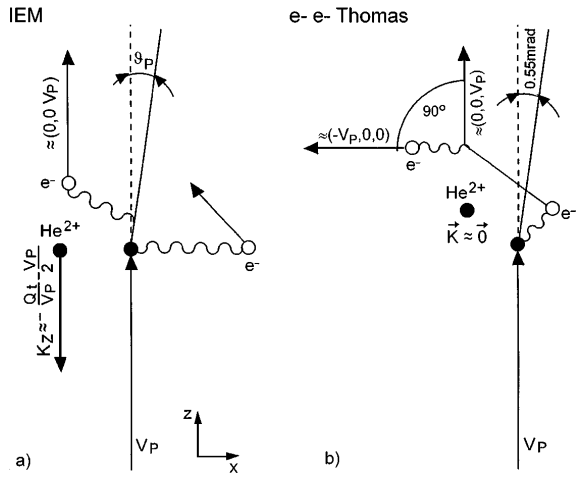

FIG. 1. Kinematics of the two-step process of kinematic capture and ionization by independent projectile electron interactions (IEM) (a) and of the correlated e-e Thomas process (b).

$$K_z = \frac{E_e - Q}{v_P} - \frac{v_P}{2} - k_z, \tag{2}$$

$Q = \epsilon_{\mathrm{He}} - \epsilon_{\mathrm{H}}$, where ϵ_{H} is the binding energy of the hydrogen atom and $\epsilon_{\mathrm{He}}(= -2.9$ a.u.) is that of the helium ground state. E_e is the final continuum energy of the emitted electron. The capture leads predominantly to the ground state of hydrogen ($Q = -2.4$ a.u.) [8]. Furthermore, rotational symmetry allows us to define $q_y = 0$ for each collision event, which means we rotate the electron and the recoil ion transverse coordinates from the lab system into the scattering plane, defined by the incident and scattered projectile. Thus x and y denote the components parallel and perpendicular to the projectile scattering plane. If we neglect Q/v_P, the signature for the strict e-e Thomas mechanism is

$$\mathbf{q} = (v_P, 0, 0), \ \mathbf{k} = (-v_P, 0, 0) \quad \text{and} \quad \mathbf{K} = (0, 0, 0), \tag{3}$$

where $q_x = v_P$ corresponds to $\theta_P = 0.55$ mrad.

Figure 2 shows the longitudinal recoil ion momentum distribution for $E_P = 0.5$, 0.8, and 1.2 MeV, each at $\theta_P = (0.15 \pm 0.15)$ and (0.55 ± 0.15) mrad as indicated in the figure, i.e., the doubly differential cross section $d\sigma/(d\theta_P dK_z)$. The full curve represents an IE approximation which divides the two-electron transition into two independent one-electron transitions for transfer and ionization. The transfer amplitude was calculated in the continuum distorted wave (CDW) formalism and the ionization amplitude in the first Born approximation [5,15]. The calculated results are scaled by a factor of 0.5 for $E_P = 0.5$ and 0.8 MeV. In this model, Eq. (2) may be split into two contributions which can be assigned to the different processes,

$$K_z = \underbrace{-\frac{Q_t}{v_P} - \frac{v_P}{2}}_{\text{transfer } (K_0)} + \underbrace{\frac{E_e - Q_i}{v_P}}_{\text{ionization}} - k_z, \tag{4}$$

with $Q_t + Q_i = Q$. The first contribution $K_0 = -Q_t/v_P - v_P/2$ results from the capture and leads to a backward momentum transfer to the recoil ion which is independent of the continuum electron momentum $\mathbf{k}$, while the second contribution represents the momentum transfer to the recoil ion originating from the ionization process only. We chose $Q_t = -1.5$ a.u. and $Q_i = -0.9$ a.u. which correspond to the assumption that the more loosely bound electron is ionized. The left vertical lines in Figs. 2(a)–2(f) show the values of K_0 for the different projectile velocities.

The IEM results are nearly symmetric around K_0 for all E_P, which is understandable because the IE model leads to $K_z \approx K_0$ whenever $E_e \ll v_P$ or $k_z \approx (E_e - Q_i)/v_P$. The latter case corresponds to the binary ridge condition. At $\theta_P = 0.15$ mrad, the present experiment shows a backward emission of the recoil ions. This backward momentum increases with increasing velocity, but not as much as the IE model predicts. The discrepancy between the IEM and the experiment becomes bigger with increasing velocity. At $\theta_P = 0.55$ mrad up to $E_P = 0.8$ MeV, the main peak of the experiment shows a much better agreement with the IE approximation than for $\theta_P = 0.15$ mrad. At $E_P = 0.5$ MeV, a shoulder and, at 0.8 MeV, a distinct peak structure appear close to $K_z = 0$. At 1.2 MeV, the doubly differential cross section is already dominated by recoil ions near $K_z = 0$. These facts cannot be described by the IEM; thus the contribution around $K_z = 0$ is assigned to the *e-e* Thomas mechanism [see also Eq. (3)]. The slightly positive K_z of the Thomas contribution may result from the neglected Q value.

Figure 3 shows the triply differential cross section $d^3\sigma/(d\theta_P dK_x dK_z)$ for $\theta_P = (0.55 \pm 0.15)$ mrad at proton energies of [3(a)] 0.5 MeV and [3(b)] 1 MeV. Figure 3(c) represents the dCTMC calculation for (0.55 ± 0.1) mrad at 1 MeV without and [3(d)] with the *e-e* interaction (*e-e* dCTMC). At 0.5 MeV [3(a)] most of the ions are found very close to K_0 (dashed line), while at 1 MeV [3(b)] the momentum distribution shows two distinct peaks, one at $K_x = -1.6$ a.u. and $K_z = -2.8$ a.u., and one at $K_x = -0.4$ a.u. and $K_z = 0.7$ a.u. The main peak at 0.5 MeV, as well as the lower peak at 1 MeV, shows the clear signature of kinematic capture plus independent ionization. The upper peak in Fig. 3(b) again corresponds to the *e-e* Thomas mechanism. The kinematic capture plus independent ionization results in a much larger K_x than the *e-e* Thomas contribution because a kinematic capture favors close impact parameters due to the high momentum components required in the initial state. Since the *e-e* Thomas mechanism does not depend on close impact parameters (it is also possible with two electrons at rest), it results mainly in small transverse recoil ion momenta. The four-body dCTMC calculations include the radial correlation between electrons by a dynamic screening parameter of the target nuclear charge as well as higher orders in the interaction between electrons and the

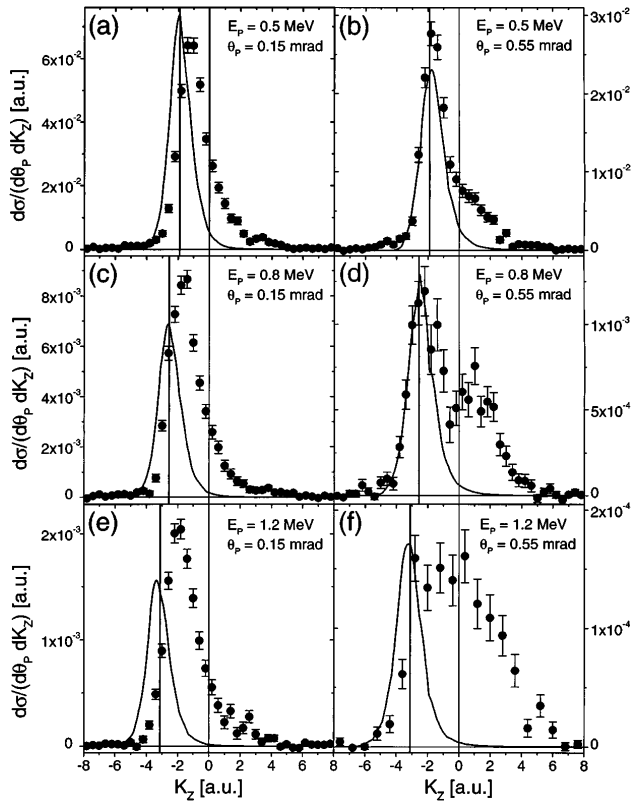

FIG. 2. Doubly differential cross section $d\sigma/(d\theta_P dK_z)$ as a function of K_z for $E_P = 0.5$ [(a), (b)], 0.8 [(c), (d)], and 1.2 MeV [(e), (f)]. (a), (c), and (e) are for $\theta_P = (0.15 \pm 0.15)$ mrad and (b), (d), and (f) are for $\theta_P = (0.55 \pm 0.15)$ mrad. Circles: present experiment; full curve: CDW-Born IEM (scaled by 0.5 for $E_P = 0.5$ and 0.8 MeV); left vertical lines: $K_z = K_0$ [see Eq. (4)].

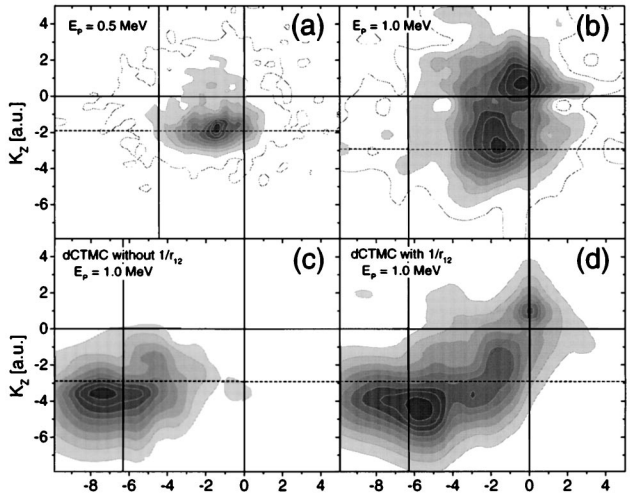

FIG. 3. Contour plot of the TDCS $d^3\sigma/(d\theta_P dK_x dK_z)$ as a function of K_x and K_z at a scattering angle of $\theta_P = 0.55$ mrad. (a),(b) Present experiment at $E_P = 0.5$ MeV (a) and 1 MeV (b). (c),(d) dCTMC calculation without (c) and (d) *e-e* interaction, both at 1 MeV. The dashed lines correspond to $K_z = K_0$ [see Eq. (4)] and the left vertical lines to $K_x = -q_x$ [see Eq. (1)].

target nucleus (i.e., the e-N Thomas mechanism). The e-e dCTMC includes the explicit $1/r_{12}$ potential which is "turned on" exponentially when the total energy of either electron relative to the He nucleus becomes positive, to enable e-e scattering but avoiding autoionization [16]. We find in the calculations without the $1/r_{12}$ interaction [Fig. 3(c)] that the longitudinal distribution shows the signature of independent capture and ionization, where the transverse momentum of the recoil ion effectively balances that of the projectile [$\theta_P = (0.55 \pm 0.1)$ mrad is equivalent to $q_x = (6.3 \pm 1.2)$ a.u.]. In Fig. 3(d), where the $1/r_{12}$ e-e interaction is now turned on, the independent process peaks again near $K_x = -6.3$ a.u., in contrast to the experiment. However, a new contribution distinct from the above appears at about $K_x = 0$ and $K_z = 1.0$ a.u. This peak, as in the experiment, is attributed to the e-e Thomas mechanism.

We have extracted the absolute contribution of the e-e Thomas scattering by folding two Gaussian fits in the singly $d\sigma/dK_z$ and doubly differential cross sections $d\sigma^2/(d\theta_P dK_z)$ [see Figs. 2(b), 2(d), and 2(e)]. The results are shown in Fig. 4. We find a $v_P^{-7.4\pm1.0}$ dependence for the e-e Thomas process by fitting the function $\sigma = a \times v_P^b$ to the data. This is in disagreement with the classical prediction of Thomas [1] and the asymptotic result of the BK2 [6,17], all predicting a v_P^{-11} dependence. However, we find a good agreement for the e-e double scattering with a "post" version of the four-body reformulated impulse approximation (RIA-4B) [19]. Among other required terms, the crucial $1/r_{12}$ interaction is explicitly included in the perturbation potential. In the exit channel, a dynamic screening of the target nuclear charge is used as a function of both the ejected electron momentum and the incident velocity.

In conclusion we have performed a kinematically complete experiment on the proton on helium transfer ionization using COLTRIMS. It enables us to distinguish clearly between the independent two-step process and the e-e Thomas scattering in the nine-dimensional momentum space of the final state. From this we obtained the first data on the absolute contribution of the Thomas process to the TI cross section between 0.5 and 1.4 MeV. COLTRIMS will also be applied to extend this experiment up to 10 MeV and to search for double Thomas structures [20,21] in He^{2+} on He double capture, at the CRYRING of the Manne-Siegbahn Institute in Stockholm. The gas target and the recoil ion momentum spectrometer for such storage ring experiments are in preparation.

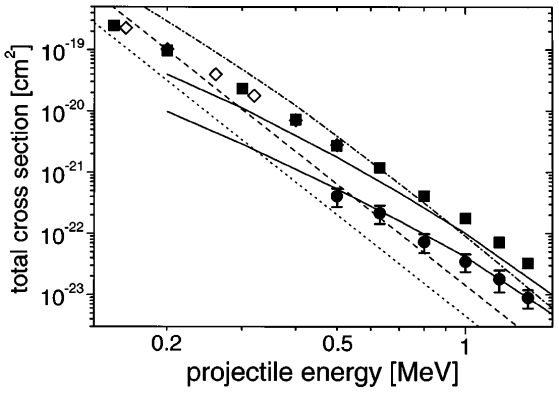

FIG. 4. Total cross section for TI: present experiment (solid squares), [18] (open diamonds), CDW-Born IEM (dashed-dotted line), and RIA-4B (upper solid line). Second-order e-e Thomas scattering: present experiment (solid circles), classical e-e double scattering [1] (dotted line), BK2 for e-e Thomas [6] (dashed line), and RIA-4B (lower solid line).

This work was supported by DFG, BMBF, GSI and EG. V. M. acknowledges support by the Studienstiftung des Deutschen Volkes, Kh. K. by the DAAD, R. E. O. by the DOE Office of Fusion Energy and the Alexander von Humboldt Foundation, Dž.B. by the Wenner-Gren Science Foundation, and C. L. C. by the Max Planck Forschungspreis. We thank our colleagues and friends, Reiner Dreizler, Stefan Keller, Jan-Michael Rost, Joachim Burgdörfer, Reinhold Schuch, and Jim McGuire, for many helpful discussions.

*Electronic address: mergel@ikf.uni-frankfurt.de
†Present address: Lawrence Berkeley Laboratory, 1 Cyclotron Road, Berkeley, California 94720.
‡Present address: University of Nevada, Reno, Nevada 89557.

[1] L. H. Thomas, Proc. R. Soc. London A **114**, 561 (1927).
[2] J. Berakdar, Ph.D. thesis, Universität Freiburg, 1992 (unpublished).
[3] E. Horsdal, B. Jensen, and K. O. Nielsen, Phys. Rev. Lett. **57**, 1414 (1986).
[4] J. Palinkas *et al.*, Phys. Rev. Lett. **63**, 2464 (1989).
[5] R. Gayet and A. Salin, Nucl. Instrum. Methods Phys. Res., Sect. B **56/57**, 82 (1991); Dž. Belkić, R. Gayet, and A. Salin, Comput. Phys. Commun. **32**, 385 (1984).
[6] J. S. Briggs and K. Taulbjerg, J. Phys. B **12**, 2565 (1979).
[7] T. Ishihara and J. H. McGuire, Phys. Rev. A **38**, 3310 (1988); J. H. McGuire *et al.*, Phys. Rev. Lett. **62**, 2933 (1989).
[8] R. Gayet and A. Salin, J. Phys. B **20**, L571 (1987).
[9] R. Dörner *et al.*, Phys. Rev. Lett. **72**, 3166 (1994).
[10] J. Ullrich *et al.*, Comments At. Mol. Phys. **30**, 285 (1994).
[11] V. Mergel *et al.*, Phys. Rev. Lett. **74**, 2200 (1995).
[12] V. Mergel, Ph.D. thesis, Universität Frankfurt/Main, ISBN 3-8265-2067-X, 1996 (unpublished).
[13] E. Horsdal-Pedersen, C. L. Cocke, and M. Stöckli, Phys. Rev. Lett. **50**, 1910 (1983).
[14] J. H. McGuire, N. C. Deb, and Y. Aktas, Phys. Rev. A **38**, 3333 (1988).
[15] A. Salin, J. Phys. B **22**, 3901 (1989).
[16] R. Moshammer *et al.*, Phys. Rev. Lett. **77**, 1242 (1996).
[17] R. Shakeshaft and L. Spruch, Rev. Mod. Phys. **51**, 369 (1979).
[18] M. B. Shah and H. B. Gilbody, J. Phys. B **18**, 899 (1985).
[19] Dž. Belkić, Nucl. Instrum. Methods Phys. Res., Sect. B **99**, 218 (1995); Phys. Scr. **53**, 414 (1996).
[20] A. E. Martinez *et al.*, J. Phys. B **27**, L375 (1994).
[21] Dž Belkić, I. Mančev, and M. Mudrinić, Phys. Rev. A **49**, 3646 (1994).